Research on Chemical Intermediates (2020) 46:1771–1788
https://doi.org/10.1007/s11164-019-04062-1

One-step biological synthesis of cauliflower-like Ag/MgO nanocomposite with antibacterial, anticancer, and catalytic activity towards anthropogenic pollutants

M. Jayapriya[1] · K. Premkumar[2] · M. Arulmozhi[1] · K. Karthikeyan[2]

Received: 3 September 2019 / Accepted: 18 December 2019 / Published online: 4 January 2020

Abstract

The present research work explores an environmental benign, lucrative approach for the synthesis of cauliflower-like Ag/MgO nanocomposite using *Musa paradisiaca* bract extract (MPBE) with multifunctional efficiency towards antibacterial, anticancer, and catalytic degradation towards methylene blue (MB), methyl orange (MO), and O-nitrophenol (O-Nip). The UV–visible absorption spectra of the synthesized Ag/MgO nanocomposite exhibit absorption peak at 270 nm and 410 nm, respectively. Fourier transform infrared spectroscopy was used to probe the functional biomolecules responsible for the reduction of Ag/MgO nanocomposite. The X-ray diffraction spectroscopy and the surface morphological images revealed the successful formation of cauliflower-like Ag/MgO nanocomposite. The fabricated nanocomposite exhibited potent antibacterial and anticancer activity for human pathogenic organisms *Escherichia coli* and *Staphylococcus aureus* with zone of inhibition 15 mm and 14 mm and showed IC_{50} value of 190 µg/ml against A549 cells. Apoptosis assay (AO/EB staining) was carried out, and the obtained results showed that bright green fluorescence indicates early apoptosis, red to orange fluorescence indicates late apoptosis, and red fluorescence denotes necrosis. Also the synthesized Ag/MgO nanocomposite exhibits enhanced catalytic degradation of 91%, 95%, and 98% in 6 min, 9 min, and 10 min for MB, MO, and O-Nip. Hence, this study highlights the use of MPBE for effective fabrication of cauliflower-like Ag/MgO nanocomposite with multifaceted application that acts as a potential candidate to resolve the diverse problems.

Keywords Ag/MgO nanocomposite · Catalytic activity · Cauliflower shaped nanocomposite · Anticancer activity · Antibacterial activity

✉ M. Arulmozhi
arulmozhiphd@hotmail.com

[1] Department of Petrochemical Engineering, Anna University-BIT Campus, Tiruchirappalli 620024, India

[2] Department of Biomedical Science, Bharathidasan University, Tiruchirappalli 620024, India

Introduction

Recent progress in utilizing inorganic nanoparticles for multifaceted applications has garnered greater attention due to their enhanced potential towards catalyst [1, 2], antimicrobial agent [3, 4], drug delivery [5, 6], molecular diagnosis [7], and anticancer agent [8]. Among them, magnesium oxide nanoparticles (MgO NPs) are functional metal oxides that have been utilized for treating several ailments owing to its biocompatibility and significant stability under arduous conditions [9]. MgO NPs have enhanced potential in the field of catalysis, refractory materials, paints, pharmaceuticals, and bioremediation [10]. In biomedical field, MgO NPs exhibit remarkable applications in bone regeneration [11], antimicrobial agent [12], antitumour agent [13], antioxidant [14], analgesic [15], anti-inflammatory [16], and antidiabetic [17]. US Food and Drug Administration acknowledged that MgO NPs (21CFR184.1431) are non-hazardous, eco-friendly in nature that can be readily used in pharmaceutical industries [18]. The plausible mechanism of MgO NPs behind the aforesaid biological activities may be due to reactive oxygen species (ROS)-induced oxidative stress that results in the formation of superoxide anions($O_2 \cdot -$), hydroxyl radicals ($\cdot OH$), dissolution of cations, etc. [19]. Also incorporation of these nanomaterials exhibits dissolution of cell membrane that results in inhibition of enzyme activity, synthesis of DNA, and disruption of energy transduction [20]. Further, ROS produced by these nanomaterials induce anticancer, antitumor, and catalytic activity that made MgO as a versatile candidate in both environmental and therapeutic applications. However, the above applications are mainly due to the controlled morphology, structure, and size because of its alterations in physical and chemical properties.

Hence to fabricate MgO nanoparticles with multifunctional efficiency, it is necessary to modify both morphology and surface chemistry as the above-mentioned applications occur on the surface of nanomaterial [10]. So the fabrication of nanoparticles with various morphologies provides reaction specificity which may be due to the formation of various surface atoms and crystallographic facets. In the recent past, there have been reports on the MgO-based metal nanoparticles that actively utilized in multifarious field. Hence, the present work intends to develop Ag/MgO nanocomposite to improve the surface morphology of MgO NPs, and thus, AgNPs are considered to have capacious spectrum of catalytic, antimicrobial, anticancer, and anti-inflammatory activities [21–24]. Also the fascinating properties of AgNPs are that at minimum concentration it is lethal to microbes but safe to human beings. Our previous report showed that biologically derived AgNPs exhibit exemplary antimicrobial, antioxidant, and catalytic activity towards various anthropogenic pollutants [21, 22]. Certain studies showed that metal/metal oxide nanocomposites exhibit better bactericidal activities against several gram-positive and gram-negative bacteria [25]. There are several physiochemical strategies that have been employed to fabricate metal/metal oxide nanocomposite with various morphologies such as core–shell [26], yolk-shell [27], nano-rattle [28], nanotubes [29], nanosheets [30], and so forth. The fabrication of aforesaid nanostructure includes several physiochemical strategy that produce

harsh environmental conditions, rigorous energy, and toxic byproducts [31]. In this context, there is an increase in concern to develop a lucrative, environmental benign strategy that provides superior platform to fabricate Ag/MgO nanoparticles with well-defined morphology that acts as a potent candidate to resolve diverse problems with multifunctional properties.

Hence in this study, *Musa paradisiaca* (MPBE) bract extract was used as a reducing and capping mediator for the one-spot synthesis of Ag/MgO nanoparticles. MPBE is rich in several phytoconstituents such as flavonoids, tannins, alkaloids, and phenolic compounds, especially the bract part *M. paradisiaca* consists of anthocyanins like delphinidin, peonidin, malvidin, and pelargonidin which are notorious for their antimicrobial, anticancer, and antioxidant properties [32, 33]. Also these phytoconstituents are responsible for the reduction of several metal and metal oxide nanoparticles. Herein, biological method was adopted for the fabrication of Ag/MgO nanocauliflower using MPBE as a reducing and capping mediator. To the best of our knowledge, this is the first report that employs eco-friendly method for the fabrication of Ag/MgO nanocomposite that provides simple, cost-effective approach that revokes harsh environmental conditions and hazardous chemicals. Then, the synthesized nanocomposite were characterized using UV–visible spectroscopy, Fourier transform infrared (FT-IR) spectroscopy, X-ray diffraction (XRD) spectroscopy, field emission scanning electron microscopy (FE-SEM), transmission electron microscopy (TEM), and X-ray fluorescence (XRF) spectroscopy. Further, the synthesized Ag/MgO nanocomposite was investigated for its multifunctional efficiency towards antibacterial, cytotoxicity of Ag/MgO nanocomposite towards lung cancer cell line and catalytic degradation of methyl orange (MO), methylene blue (MB), and O-nitro phenol (O-nip) (Scheme 1).

Experimental

Materials

Magnesium nitrate hexahydrate (Mg $(NO_3)_2{\cdot}6H_2O$) and silver nitrate ($AgNO_3$) were obtained from Sigma-Aldrich, India. Muller Hinton Agar (MHA), MHA broth, 3-[4,5-dimethylthiazole-2-yl]-2,5-diphenyltetrazolium bromide (MTT), and sterile

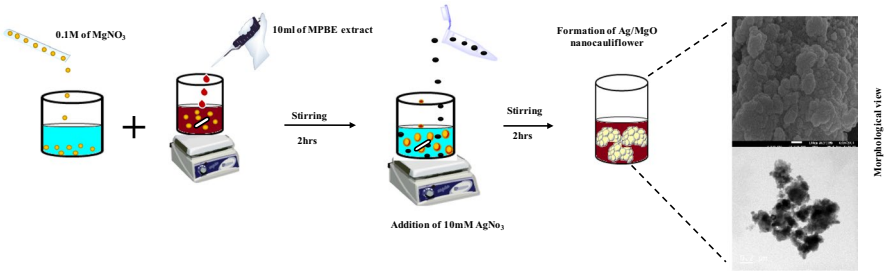

Scheme 1 Schematic illustration for the formation of Ag/MgO nanocauliflower

discs. Dulbecco's Modified Eagle's medium (DMEM) was obtained from Himedia laboratories, India. Other chemical agents used in the current study were of analytical grade and used without purification. *M. paradisiaca* bract was procured from local market, Tiruchirappalli, Tamil Nadu, India. Double-distilled water ($DD{\cdot}H_2O$) was used throughout the experiment.

Preparation of MPBE extract

MPBE extract was prepared by taking 1:10(w/v) proportion of finely chopped bract and $DD.H_2O$. The aforesaid mixture was boiling at 60 °C for 30 min under reflux conditions. Then, the dispersion was decanted using Whatmann No. 1 filter paper to separate the solid particles. The distillate was stored at 4 °C and used as a reducing and capping mediator for the fabrication of nanocomposite.

Synthesis of Ag/MgO Nano cauliflower

Environmental benign strategy was employed to fabricate Ag/MgO nanocauliflower. In a typical synthesis, 10 ml of MPBE was added slowly to 100 ml of 0.1 M $(MgNO_3)_2{\cdot}6H_2O$) solution and stirred continuously for 2 h at room temperature. Then, 10 mM of $AgNO_3$ was added to the above-mentioned suspension. The reaction mixture was stirred vigorously for about 4 h. The resulting precipitate was centrifuged and washed several times with $D{\cdot}DH_2O$, ethanol, and acetone to rule out impurities. The obtained precipitate was dried in room temperature and calcined at 300 °C for 2 h.

Characterization studies

The UV–visible absorption spectrum of synthesized nanocomposite was carried out using JASCO-V700 series spectroscopy in the range of 200–800 nm. The functional groups responsible for the reduction of Ag/MgO nanoparticles were screened using FT-IR spectroscopy in the range of 400–4000 cm^{-1} (Perkin Elmer, UK, Paragon-500). XRD pattern of synthesized nanocomposite was examined using X'pert Pro diffractometer (Pan Analytical) System with CuK radiation ($K = 1.5406$ Å). The morphological investigation of the synthesized nanocomposite was analysed using FE-SEM, (JOEL JSM-7600F FEG-SEM), and the elemental analysis was carried out using XRF (Shimadzu Ltd., LAB CENTER XRF-1800 Tokyo, Japan). Further topographical and morphological investigation was carried out using TEM, Philips CM 200, operating at a voltage 200 kV.

Antibacterial activity

The antibacterial activities of the synthesized Ag/MgO nanocomposite were assessed using disc diffusion method. The bacterial strains of gram-positive *Staphylococcus aureus* (*S. aureus*) and gram-negative *Escherichia coli* (*E. coli*) were used as a model test strains. In vitro antibacterial activity was examined using Muller

Hinton Agar (MHA) medium obtained from Himedia laboratory (Mumbai). Fifteen millilitre of MHA molten agar medium was poured into a sterile Petri plates and allowed to solidify for 5 min. The inoculum suspension was swabbed homogeneously and dried for 5 min. Then, 60 µl of Ag/MgO nanocomposite was loaded on 6 mm sterile disc. Further, nanocomposite-loaded disc was placed on the surface of the medium, and then, the plates were incubated at 37 °C for 24 h. Standard antibiotic disc ciprofloxacin (CIP) was used as a positive control. After incubation, zone of inhibition was measured with transparent ruler in millimetre.

In vitro anticancer activity of synthesized Ag/MgO nanocomposite

Cell culture

Human lung cancer cell line (A549) was procured from National Centre for Cell Science (NCCS), Pune, India. The A549 cells were cultured in DMEM medium consisting of 10% foetal bovine serum (FBS) and 1X antibiotic solution (10,000 units penicillin and 10 µg/ml streptomycin) kept in a humidified atmosphere incubated at 37 °C with 5% CO_2.

Cytotoxicity assay

Cytotoxicity of synthesized Ag/MgO nanocomposite against A549 cell line was measured using MTT assay. Typically cultured A549 cells (1×10^6 cells/ml) were added on 96-well plates and exposed with different concentration of Ag/MgO nanocomposite (100–200 µg/ml), and the plates were incubated at 37 °C for 24 h with atmosphere containing 5% CO_2. The incubated cells were then treated with 10 µl of MTT and further incubated for about 4 h at 37 °C with 5% CO_2 atmosphere. Then, the formazan crystals were dissolved well with 200 µl of DMSO and the absorbance was measured colorimetrically at 570 nm. The effect of synthesized Ag/MgO nanocomposite on the proliferation of A549 cell line was measured using the formula given below.

$$\%\text{of viability} = \frac{\text{OD value of experimental sample}}{\text{OD of control samples}} \times 100$$

Apoptosis assay

Acridine orange/ethidium bromide (AO/EB) staining was used to examine the Ag/MgO nanocomposite-induced apoptosis in A549 cancer cell line. Cultured A549 cells (1×10^6 cells/ml) were seeded in 6-well plates and treated with opted IC_{50} concentration of Ag/MgO nanocomposites. Then, the plates were incubated at 24 h and 48 h at 37 °C with the atmosphere containing 5% CO_2. After the period of incubation, AO/EB staining solution was added and incubated for 5 min. The unbinded dyes were removed by washing with PBS. The stained cells were examined under

UV illumination using the 40× objective (Nikon 80i Eclipse, Japan), and the digitized images were captured for the identification of apoptotic cell death.

Catalytic activity of Ag/MgO nanocauliflower

MO, MB, and O-nip were chosen as a model reaction to evaluate the catalytic efficiency of biologically fabricated Ag/MgO nanocauliflower. The reaction was carried out in standard quartz cuvette of 1 cm path length with 4 ml volume. Briefly, aqueous solution of O-nip (30 µl of 0.01 M) was mixed well with 1.5 ml of D·DH_2O and 1 mg of solid $NaBH_4$ was added to the aforesaid mixture followed by the addition of 5 mg of Ag/MgO nanocauliflower. Similarly, 1 mM of MO or 2 mM of MB was mixed well with 1 ml of D DH_2O followed by the addition of freshly prepared $NaBH_4$ (0.5 M, 200 µl) solution and catalysts to the reaction mixture. The reduction process was monitored using UV–visible spectroscopy.

Results and discussion

UV–visible spectroscopy

The UV–visible absorption spectra of the synthesized Ag/MgO nanocomposite exhibit characteristic absorption peak at 270 nm and 410 nm, respectively (Fig. 1). The existence of two distinct absorption peak confirms the formation of Ag/MgO nanocomposite. The absorption peak at 270 nm corresponds to n–π^* transition which may be attributed to the excitation of surface O_2^- anions of MgO nanoparticles and the peak at 410 nm corresponds to π–π^* which may be due to the surface plasmon resonance of AgNPs. The synthesized AgNPs exhibit shorter wavelength (410 nm) which confirms the formation of Ag NPs with reduced size which was consistent with previous report [34, 35]. The obtained results was consistent with the previous report.

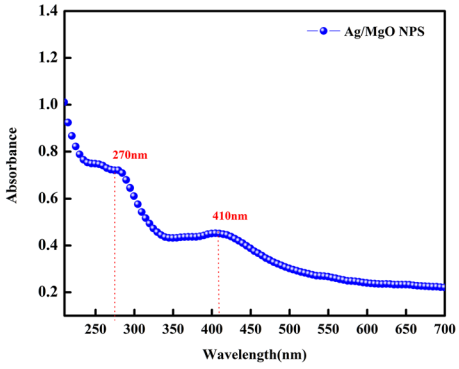

Fig. 1 UV–visible spectrum of synthesized Ag/MgO nanocomposite

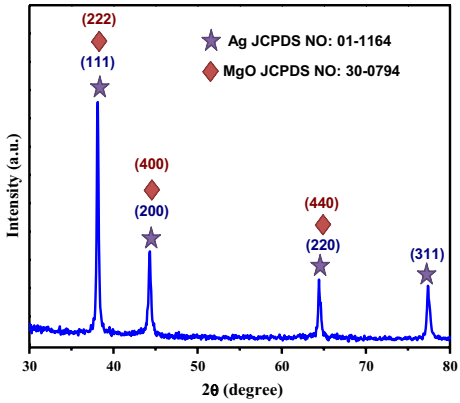

Fig. 2 Powder XRD pattern of Ag/MgO nanocomposite

X-ray diffraction (XRD) analysis

The X-ray diffraction pattern of the synthesized Ag/MgO nanocomposite is shown in Fig. 2. The diffraction peaks at $2\theta = 38°$, 44°, 63° can be indexed to the *hkl* planes (222), (400), and (440) corresponding to cubic MgO phase (JCPDS 30-0794) [34]. Similarly, the diffraction peaks at Ag observed at 2θ positions 38°, 44°, 63°, and 78° indexed to (111), (200), (220), and (311) crystallographic plane of cubic Ag phase (JCPDS 01-1164), respectively [35].

The average crystalline size of the synthesized Ag/MgO nanocomposite was obtained using Scherrer equation,

$$D = K\lambda/\beta\cos\theta$$

where D is the average particle size, K is the shape factor (constant 0.9), λ is the X-ray wavelength (1.5406 Å), β is the full width at half maximum of the peak (FWHM), and θ is the diffraction angle and found to be 45 nm.

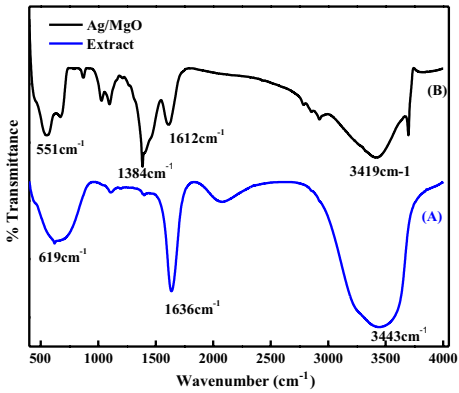

Fig. 3 Fourier transform infrared (FT-IR) spectrum of **a** MPBE extract, **b** Ag/MgO nanocomposite

FT-IR analysis

FT-IR analysis was performed to identify the biomolecules responsible for the reduction of Ag/MgO nanocomposite. Figure 3a shows the broad stretch at band positions 3443, 1636, and 619 cm^{-1}. The vibration band obtained at 3443 and 1636 cm^{-1} corresponds to N–H, N=C=S vibrations and –C=C– vibrations, respectively. These vibrations assigned to the phytochemicals present in the MPBE extract [10, 21]. The same vibrations with reduced intensity were observed in the Ag/MgO nanocomposite. The functional group vibrations shift may be attributed to the surface functionalization of phytochemicals of Ag/MgO nanocomposite. The broadband between 400 to 600 cm^{-1} corresponds to the Ag and MgO nanoparticles [36]. The reduction of Ag/MgO nanocomposite by MPBE extract may be due to the presence of phytoconstituents, namely alkaloids, tannins, flavonoids, phenolic compounds, and anthocyanins. The reduction of MgO nanoparticles may be attributed to p-track conjugation effect formed by the lactone hydrogen atom and the hydroxyl group present in the polyphenol. By the process of chelating effect, the hydroxyl group binds with metal ions to form metal phenolate complex. Further, it undergoes hydrolysis to form metal oxide nanostructure. The formation of Ag NPs due to the tautomeric conversion of anthocyanin from enol to keto form may liberate an active hydrogen atom that can reduce metal ions to form AgNPs.

Morphological analysis

The morphological and topographical view of the synthesized Ag/MgO nanocomposite was visualized using electron microscopy. The FE-SEM image of the synthesized Ag/MgO nanocomposite revealed the formation of cauliflower-shaped nanoparticles which may due to the orientation attachment and aggregation of Ag and MgO nuclei which is clearly depicted in Fig. 4a, b. Further, the formation of cauliflower-shaped nanocomposite was substantiated using TEM analysis where an average diameter ~ 100 nm is shown in Fig. 4b [37]. Further, the chemical purity of the synthesized Ag/MgO nanocomposite was investigated using XRF studies. Figure 5 reveals the presence of elemental signals of Ag and Mg which confirms the presence of silver on the surface of magnesium, and the intensity of oxygen was lower than that of aforesaid materials. The presence of weak signals affirms the carbon and oxygen peaks which clearly showed the capping of biomolecules present in MPBE extract.

Antibacterial activity

The antibacterial activity of the as-synthesized Ag/MgO nanocomposite using MPBE was evaluated using disc diffusion method against *E. coli* and *S. aureus* and the positive control ciprofloxacin. Figure 6a, b shows the potent bactericidal activity against both gram-negative and gram-positive bacteria. *Escherichia coli* showed maximum inhibition zone of 15 mm, and *S. aureus* showed 14 mm at

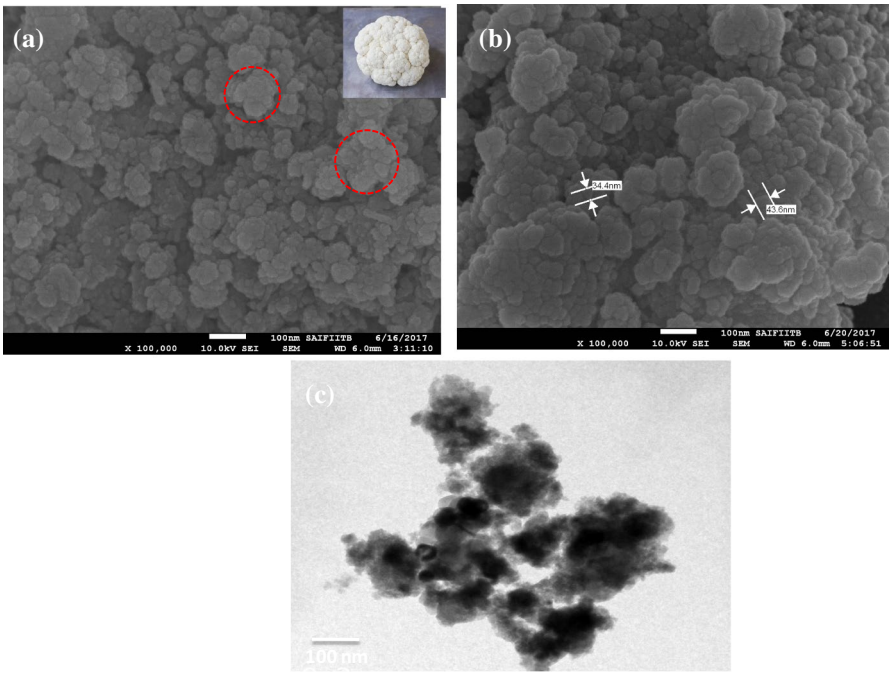

Fig. 4 **a** FE-SEM image of fabricated Ag/MgO nanocauliflower and **b** TEM view of Ag/MgO nanocauliflower

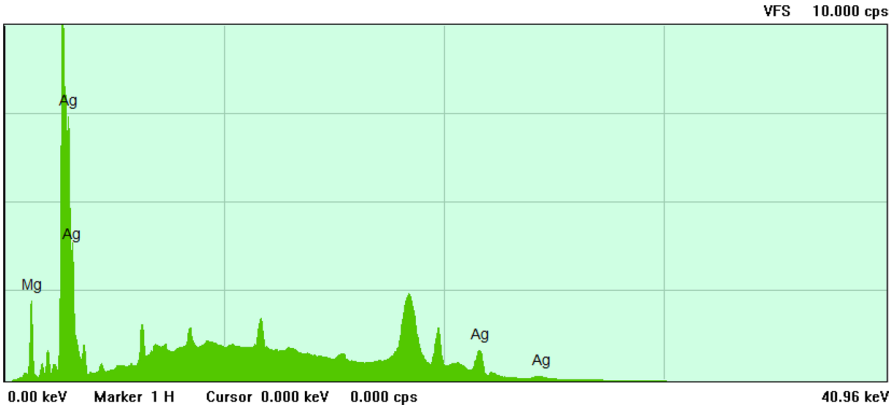

Fig. 5 Elemental analysis of Ag/MgO nanostructures using XRF study

the concentration of 60 µl (mg/ml), respectively [38]. The enhanced antibacterial activity of the synthesized Ag/MgO nanocomposite may be due to the formation of more defect sites on the surface of MgO that intensifies the adsorption of oxygen to produce more reactive oxygen species (ROS) [39].

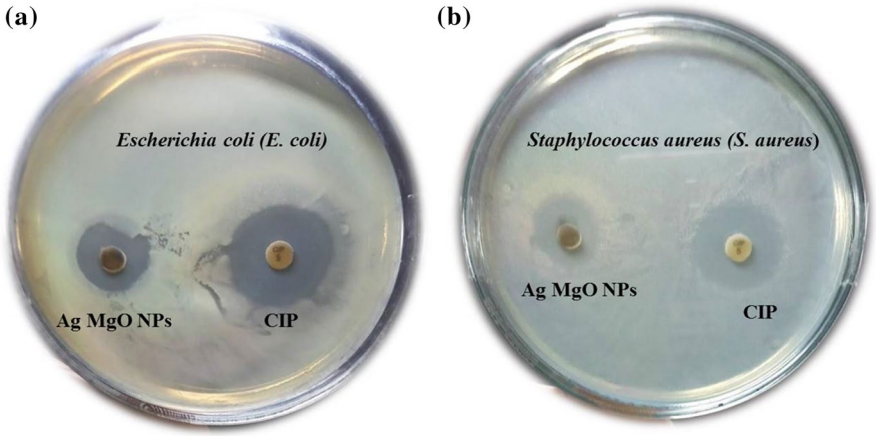

Fig. 6 Antibacterial activity of the synthesized Ag/MgO nanocomposite **a** *E. coli* and **b** *S. aureus*

Anticancer potential of Ag/MgO nanocomposite

Globally increased mortality was found due to the most prevalent form of lung carcinoma in both the sexes. Results illustrated from epidemiological studies showed that amidst all types of cancer 12.4% of new cases and 17.6% of total cancer mortality were due to lung cancer [40]. Non-small lung cancer (NSCLC) is the major patron of total lung cancer, which was further divided into adenocarcinoma (35%), large cell carcinoma (2.9%), and squamous cell carcinoma (20%) [41]. A549 cancer cells (adenocarcinomic human alveolar basal epithelial cells) were used frequently as in vitro model systems for the study of NSCLC [42]. Traditional treatment methods such as chemotherapy, surgery, and radiation therapy itself or in combination are being used for lung cancer treatment [43]. However, these methods are expensive with harsh side effects neuronal damage, skin irritation, and severe ache [44].Hence, there is need for the development of non-hazardous, environmental benign, and lucrative drug for the treatment of cancer [45]. Thus nanoparticles with the smaller size possessing unique physiochemical properties that provides superior platform of exceptional interactions with nucleic acids, lipids, and proteins present on the surface of the cell and the body cells present inside. Hence the nanomaterials can be used in the diagnosis and treatment of lung carcinoma. In the recent past, several metal nanoparticles such as Ag, Au, and Pt have been used in carcinoma therapy against various types of cancer [46]. In this study, the anticancer potential of Ag/MgO nanocomposite synthesized using MPBE was investigated against lung cancer cell lines (A549).

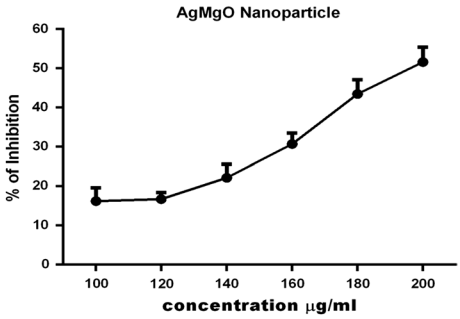

Fig. 7 In vitro cytotoxic effect of synthesized Ag/MgO nanocomposite using MTT assay

In vitro cytotoxicity

The in vitro cytotoxic effect of the synthesized Ag/MgO nanocomposite on lung cancer cell lines (A549) was evaluated using MTT assay. Figure 7 shows the cytotoxic effect of synthesized Ag/MgO nanocomposite with the reduction in the mitochondrial function of A549 cells in a dose-dependent manner with an IC_{50} value of 190 µg/ml [47]. Previous studies showed that the green-synthesized Se-NPs were evaluated for its anticancer activity against HepG2 and Mcf-7 and exhibit IC_{50} value of 392.57 and 252.44 µg, whereas the synthesized nanocomposite exhibits lower IC_{50} with higher anticancer efficiency. Hence from the obtained results, it was scrutinized that the synthesized Ag/MgO nanocomposite actively inhibits A549 cell line that acts as a potent candidate in biomedical field [48–50]

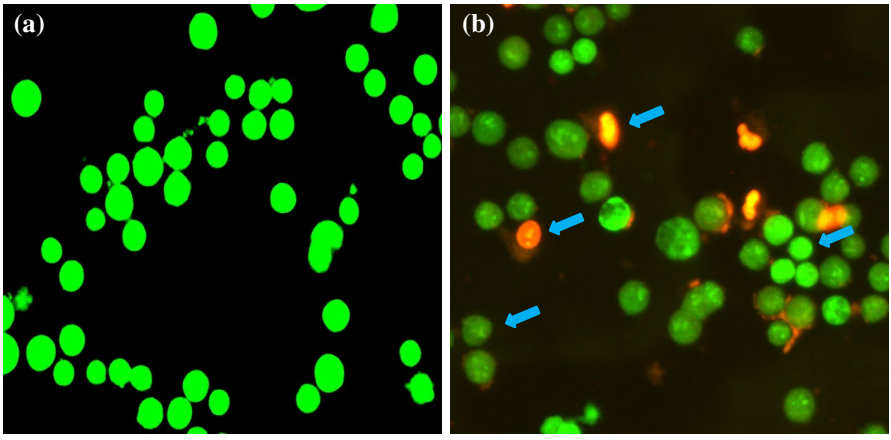

Fig. 8 Photomicrographs of AO/EB-stained A549 cells incubated for 24 h **a** without Ag/MgO NPs and **b** with Ag/MgO NPs, respectively. Cells which are viable (light green), early apoptotic (bright green fluorescence), late apoptosis (red to orange fluorescence), and necrosis (red fluorescence). (Color figure online)

Apoptosis assay in A549 cells induced by Ag/MgO nanocomposite

Provoking the apoptotic pathway for killing the cancer cells is the key point for chemotherapeutic drugs used in cancer treatment. Figure 8a, b shows the AO/EB-stained A549 lung cancer cell line treated with the synthesized Ag/MgO nanocomposite through which the morphological changes occurred during apoptosis were observed. From the obtained results, the fluorescent green represents the viable cancer cells (Fig. 8a), whereas the Ag/MgO nanocomposite-treated cancer cells (Fig. 8b) showed bright green fluorescence, indicating that early apoptosis, red to orange fluorescence indicates late apoptosis, and red fluorescence denotes necrosis. Hence from the obtained results, it was scrutinized that the Ag/MgO nanocomposite actively triggers apoptotic cell death in A549 cell line [51, 52].

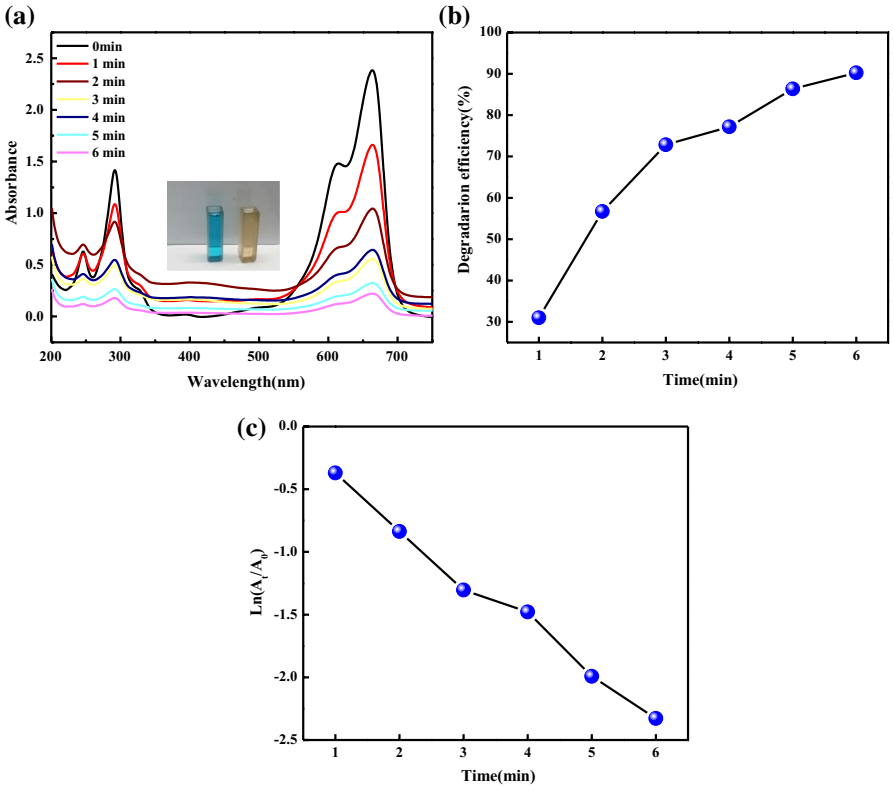

Fig. 9 **a** UV–visible absorption spectra for the degradation of MB by $NaBH_4$ in the presence of Ag/MgO nanocomposite, **b** degradation efficiency and **c** plot of $\ln(A_t/A_0)$ versus reaction time for the reduction of MB using Ag/MgO nanocomposite

Catalytic degradation of dyes

MB degradation using Ag/MgO nanocomposite

MB is a heterocyclic aromatic compound that exhibits absorption peak at 660 nm and shoulder peak at 290 nm. The peak at 660 nm attributed to the chromophore functional group of MB and its dimers, notably –C=S and –C=N, whereas the peak at 290 nm ascribed to $\pi - \pi^*$ transition belongs to unsaturated conjugate aromatic rings [50, 51]. After the addition of $NaBH_4$ and Ag/MgO Nano catalyst, the intensity of the absorption band at 660 nm and 290 nm gradually diminishes which showed the concurrent oxidation, reduction, and mineralization of the MB which is shown in Fig. 9a. The degradation efficiency of MB in the presence of Ag/MgO nanocomposite was found to be 91% in 6 min (Fig. 9b).The enhanced degradation of MB dye may be due to the formation of $O_2^{\cdot}$ and $OH^{\cdot}$ radicals owing to the amalgamated effect of Ag and MgO nanoparticles. Insert Fig. 9a depicts the visual decolourization of MB dye. The plausible mechanism for the transfer of electrons from $NaBH_4$ to excited MB and its reduction is represented by following reaction

$$\text{Ag/MgO NaBH}_4 + h\nu \rightarrow \text{Ag/MgO} - \text{NaBH}_4(h^+ - e^-)$$
$$2e^- + \text{MBH}^+ + \text{H}^+ \rightarrow \text{Respective end product}$$

The kinetics of the reaction was probed using time-dependent absorption spectrum of MB, when an excess amount of $NaBH_4$ was added to the reaction mixture compared to that of MB. Henceforth, the rate of the reaction is independent of $NaBH_4$. So the reaction followed pseudo-first-order kinetics it may be denoted as follows.

$$\ln\left(C_t/C_0\right) = \ln\left(A_t/A_0\right) = -\text{Kapp}\, t$$

where C_t = concentration at time and C_0 = concentration at $t = 0$, A_t = absorbance of dye at time t and A_0 = absorbance at $t = 0$, Kapp = apparent rate constant. Figure 9c represents the graph of ln (A_t/A_0) with radiation time for Ag/MgO From the displayed sketch, the rate constant of the reaction was found to be 6.395×10^{-3} s^{-1} for Ag/MgO nanocomposite.

MO degradation using Ag/MgO nanocomposite

MO is an azo dye that has wider application in paper dyeing, printing, and textile industries as an organic dye [53]. MO exhibits characteristic absorption peak at 463 nm in the presence of $NaBH_4$; after the addition of Ag/MgO nanocomposite, the intensity of MO was gradually reduced with respect to time (Fig. 10a). After 9 min, the degradation efficiency of MO in the presence of Ag/MgO nanocomposite was found to be 95% which is depicted in Fig. 10b. MO degradation obeys pseudo-first-order kinetics. From the graph (Fig. 10c), the rate constant of the reaction was found

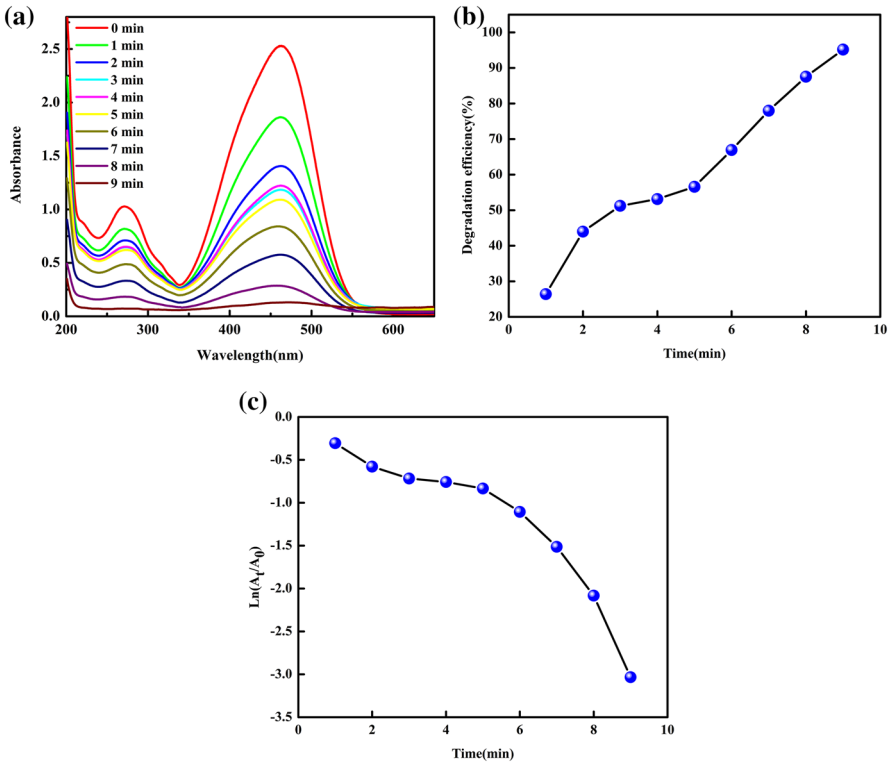

Fig. 10 **a** UV–visible absorption spectra for the degradation of MO by $NaBH_4$ in the presence of Ag/MgO nanocomposite, **b** degradation efficiency, and **c** plot of $\ln(A_t/A_0)$ versus reaction time for the reduction of MO using Ag/MgO nanocomposite

to be 4.83×10^{-3} s^{-1}. Insert Fig. 10a shows the visual reduction of MO dye. The plausible mechanism for the transfer of electrons from $NaBH_4$ to excited MO and its reduction is represented by following reaction.

$$\mathrm{Ag/MgO - NaBH_4} + h\nu \rightarrow \mathrm{Ag/MgO - NaBH_4}\left(h^+ - e^-\right)$$

$$2e^- + \mathrm{MOH^+} + \mathrm{H^+} \rightarrow \text{Respective end product.}$$

O-Nip degradation using Ag/MgO nanocomposite

The compiled UV-absorption spectra of O-Nip in the presence of Ag/MgO nanocomposite is shown in Fig. 11a. The absorption spectra of O-Nip were exhibited at 340 nm. Subsequently after the addition of $NaBH_4$, there is a peak shift from 340 to 415 nm that reveals the formation of nitrophenolate ions. After the addition of Ag/MgO nanocomposite, the absorption peak at 415 nm gradually reduces which was visually confirmed by the change of colour from yellow to colourless solution (insert Fig. 11a).The degradation efficiency of O-Nip in the presence of Ag/MgO nanocomposite was found to be

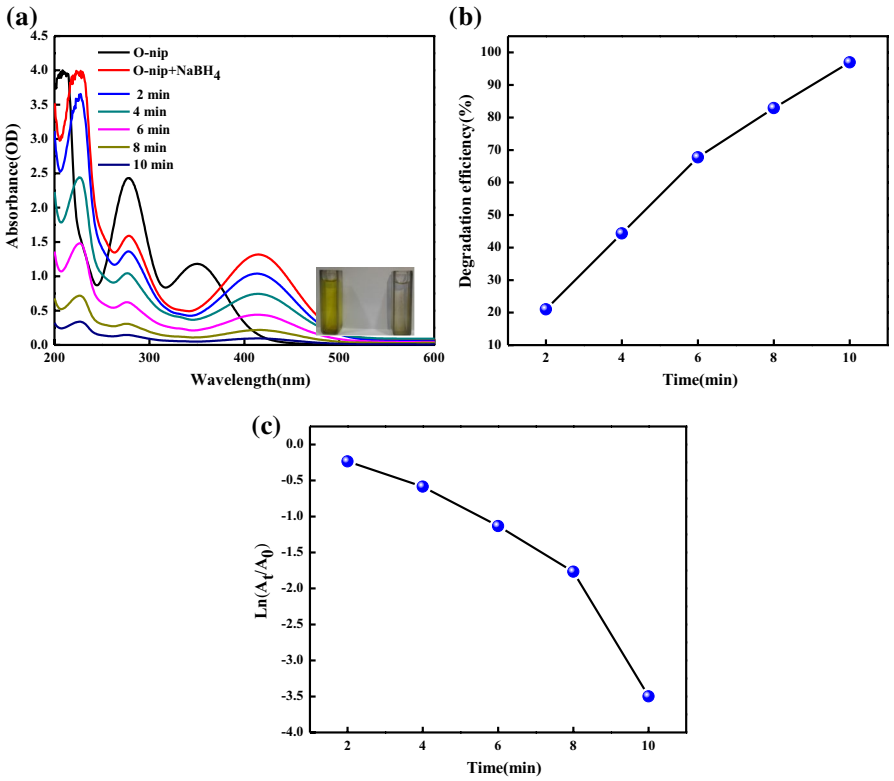

Fig. 11 **a** UV–visible absorption spectra for the degradation of O-nip by $NaBH_4$ in the presence of Ag/MgO nanocomposite, **b** degradation efficiency and **c** plot of $\ln(A_t/A_0)$ versus reaction time for the reduction of O-nip using Ag/MgO nanocomposite

98% in 10 min is depicted in Fig. 11b. From the graph (Fig. 11c), the rate constant of the reaction was found to be 6.421×10^{-3} s^{-1} which obeys pseudo-first-order kinetics [54–56].

Possible mechanism for the catalytic degradation of pollutants

The possible mechanism for the catalytic degradation of aforestated organic pollutants and azo dyes using Ag/MgO nanocomposite may be due to the amalgamated effect of Ag on MgO and is shown in Fig. 12. Ag ions can effectively relay the electrons propagated by BH^{4-} to the anthropogenic pollutants and the adsorbed O_2 at the surface of MgO.

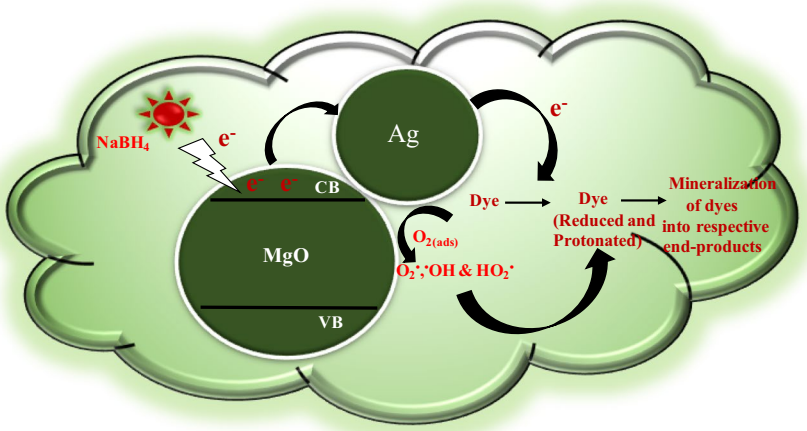

Fig. 12 Proposed mechanism for the catalytic reduction, oxidation, and mineralization of respected end products by $NaBH_4$ in the presence of Ag/MgO nanocomposite

Conclusion

In summary, this is the first ever report where cauliflower-like Ag/MgO nanocomposite was synthesized using MPBE which was considered as an environmental benign, lucrative strategy. The synthesized Ag/MgO nanocomposite acts as a multifunctional platform with potent antimicrobial, anticancer, and catalytic potential towards MO, MB, and O-Nip. The incorporation of Ag on MgO exhibits its enhanced antibacterial activity for human pathogenic organisms *E. coli* and *S. aureus* with zone of inhibition 15 mm and 14 mm [57, 58] and showed IC_{50} value of 190 µg/ml against A549 cells. Gaining insight into the anticancer activity apoptosis assay (AO/EB staining) was carried out, and the obtained results showed bright green fluorescence indicates early apoptosis, red to orange fluorescence indicates late apoptosis, and red fluorescence denotes necrosis. Also the synthesized Ag/MgO nanocomposite exhibits enhanced catalytic degradation of 91%, 95%, and 98% in 6 min, 9 min, and 10 min for MB, MO, and O-Nip. Hence from the obtained results, it was scrutinized that the synthesized cauliflower-like Ag/MgO nanocomposite that acts as a potent candidate with multifunctional efficiency could find applications in pharmaceuticals and environmental field.

Acknowledgements Authors gratefully acknowledge the SAIF, Mumbai, for providing all spectroscopic images.

References

1. A.L. Gajeng, T. Sasaki, B.M. Bhanage, Adv. Powder Technol. **28**, 1185 (2017)
2. M. Tajbakhsh, M. Farhang, A.A. Hosseini, J. Iran. Chem. Soc. **11**, 665 (2014)
3. A. Pugazhendhi, R. Prabhu, K. Muruganantham, R. Shanmuganathan, S. Natarajan, J. Photochem. Photobiol. B **190**, 86 (2019)
4. H.R. Raveesha, S. Nayana, D.R. Vasudha, J.P. Shabaaz Begum, S. Pratibha, C.R. Ravikumara, N. Dhananjaya, J. Sci. Adv. Mater. Dev. **4**, 57 (2019)
5. M. Liong, J. Lu, M. Kovochich, T. Xia, S.G. Ruehm, A.E. Nel, F. Tamanoi, J.I. Zink, ACS Nano **2**, 889 (2008)
6. A. Riedinger, M. Pernia Leal, S.R. Deka, C. George, I.R. Franchini, A. Falqui, R. Cingolani, T. Pellegrino, Nano Lett. **11**, 3136 (2011)
7. D. Kim, J. Kim, Y.I. Park, N. Lee, T. Hyeon, ACS Cent. Sci. **4**, 324 (2018)
8. F. Wang, C. Li, J. Cheng, Z. Yuan, Int. J. Environ. Res. Public Health. **13**, 1182 (2016)
9. K. Kandiah, T. Jeevanantham, B. Ramasamy, Artif. Cells Nanomed. Biotechnol. **47**, 862 (2019)
10. M. Jayapriya, M. Arulmozhi, B. Balraj, Ceram. Int. **44**, 13152 (2018)
11. D.J. Hickey, B. Ercan, L. Sun, T.J. Webster, Acta Biomater. **14**, 175 (2014)
12. N.Y.T. Nguyen, N. Grelling, C.L. Wetteland, R. Rosario, H. Liu, Sci. Rep. **8**, 16260 (2018)
13. E. Behzadi, R. Sarsharzadeh, M. Nouri, F. Attar, K. Akhtari, K. Shahpasand, M. Falahati, Int. J. Nanomed. **14**, 257 (2019)
14. N.J. Sushma, D. Prathyusha, G. Swathi, T. Madhavi, B.D.P. Raju, K. Mallikarjuna, H.S. Kim, Appl. Nanosci. **6**, 437 (2016)
15. M. Torabi, M. Kesmati, N. Pourreza, H.N. Varzi, H. Galehdari, Life Sci. **203**, 72 (2018)
16. M.J. Climent, A. Corma, S. Iborra, M. Mifsud, J. Catal. **247**, 223 (2007)
17. S. Moeini-Nodeh, M. Rahimifard, M. Baeeri, M. Abdollahi, Biol. Trace Elem. Res. **175**, 146 (2017)
18. L. Cai, J. Chen, Z. Liu, H. Wang, H. Yang, W. Ding, Front. Microbiol. **9**, 790 (2018)
19. K. Krishnamoorthy, J.Y. Moon, H.B. Hyun, S.K. Cho, S.J. Kim, J. Mater. Chem. **22**, 24610 (2012)
20. S. Podder, D. Chanda, A.K. Mukhopadhyay, A. De, B. Das, A. Samanta, J.G. Hardy, C.K. Ghosh, Inorgan. Chem. **57**, 12727 (2018)
21. M. Jayapriya, M. Arulmozhi, B. Balraj, IET Nanobiotechnol. **13**, 134 (2018)
22. M. Jayapriya, D. Dhanasekaran, M. Arulmozhi, E. Nandhakumar, N. Senthilkumar, K. Sureshkumar, Res. Chem. Interm. **45**, 3617 (2019)
23. M. Anandan, G. Poorani, P. Boomi, K. Varunkumar, K. Anand, A.A. Chuturgoon, M. Saravanan, H.G. Prabu, Process Biochem. **80**, 80 (2019)
24. Z. Bian, J. Zhu, F. Cao, Y. Lu, H. Li, Chem. Commun. Camb. **25**, 3789 (2009)
25. A. Pugazhendhi, N. Thomas, I.E. Jebakumar, K. Indira, K. Brindhadevi, Int. J. Pharm. **539**(1–2), 104 (2018)
26. S.H. Wu, C.T. Tseng, Y.S. Lin, C.H. Lin, Y. Hung, C.Y. Mou, J. Mater. Chem. **21**, 789 (2011)
27. N.T. Nguyen, J. Yoo, M. Altomare, P. Schmuki, Chem. Commun. **50**, 9653 (2014)
28. Z. Wang, G. Meng, Z. Huang, Z. Li, Q. Zhou, Nanoscale **6**, 15280 (2014)
29. A. Mahmood, N. Ngah, M.N. Omar, Eur. J. Sci. Res. **66**, 311 (2011)
30. E.A. Pazmiño-Durán, M.M. Giusti, R.E. Wrolstad, M.B.A. Glória, Food Chem. **73**, 327 (2001)
31. A. Pugazhendhi, S.S. Kumar, M. Manikandan, M. Saravanan, Microb. Pathog. **122**, 84 (2018)
32. A.H. Chowdhury, S. Ghosh, S.M. Islam, New J. Chem. **42**, 14194 (2018)
33. I.H. Chowdhury, S. Ghosh, M. Roy, M.K. Naskar, J. Sol-Gel. Sci. Technol. **73**, 199 (2015)
34. R. Hassanien, A.A.I. Abed-Elmageed, D.Z. Husein, J. Nanosci. Nanotechnol. Appl. **3**, 104 (2019)
35. P. Manzhi, R. Kumari, M.B. Alam, G.R. Umapathy, R. Krishna, S. Ojha, O.P. Sinha, Vacuum **166**, 370 (2019)
36. D. Čempel, M.T. Nguyen, Y. Ishida, T. Tokunaga, T. Yonezawa, New J. Chem **42**, 5680 (2018)
37. M. Bordbar, RSC Adv **7**, 180 (2017)
38. D. Nipane, S.R. Thakare, N.T. Khati, J. Catal. **2013**, 8 (2013)
39. X. Zhu, D. Wu, W. Wang, F. Tan, P.K. Wong, X. Wang, X. Qiao, J. Alloy. Compd. **684**, 282 (2016)
40. W.B. Ayinde, M.W. Gitari, M. Muchindu, A. Samie, Biosynthesis of ultrasonically modified Ag–MgO nanocomposite and its potential for antimicrobial activity. J. Nanotechnol. **2018**, 10 (2018)
41. L.A. Torre, R.L. Siegel, E.M. Ward, A. Jemal, Biomark. Prev. **25**, 16 (2016)
42. J.R. Molina, P. Yang, S.D. Cassivi, S.E. Schild, A.A. Adjei, Mayo Clin. Proc. **83**, 584 (2008)
43. A.J. Alberg, M.V. Brock, J.G. Ford, J.M. Samet, S.D. Spivack, Chest **143**, e1S (2013)

44. M. Reck, K.F. Rabe, N. Engl. J. Med. **377**, 849 (2017)
45. M. Forster, A. Hackshaw, T. De Pas, M. Cobo, P. Garrido, Y. Summers, A.B. Loembé, Clin Lung Cancer **120**, 27 (2018)
46. R. Seigneuric, L. Markey, D.S. Nuyten, C. Dubernet, T.A. Evelo, E. Finot, C. Garrido, Curr. Mol. Med. **10**, 640 (2010)
47. A. Sharma, A.K. Goyal, G. Rath, J. Drug Target. **26**, 617 (2018)
48. S. Sathiyavimal, S. Vasantharaj, D. Bharathi, M. Saravanan, E. Manikandan, S.S. Kumar, A. Pugazhendhi, J. Photochem. Photobiol. B **188**, 126 (2018)
49. V. Sharma, D. Anderson, A. Dhawan, Apoptosis **17**, 852 (2012)
50. C.M. Pfeffer, A.T.K. Singh, Int. J. Mol. Sci. **19**, 448 (2018)
51. T.B. Nguyen, R.A. Doong, C.P. Huang, C.W. Chen, C.D. Dong, Sci. Total Environ. **675**, 531 (2019)
52. C.M. Hung, C.W. Chen, Y.Y. Liu, C.D. Dong, Water Environ. Res **88**, 675 (2016)
53. X. Lai, R. Guo, H. Xiao, J. Lan, S. Jiang, C. Cui, E. Ren, J. Hazard. Mater. **371**, 506 (2019)
54. E. Nandhakumar, P. Priya, R. Rajeswari, V. Aravindhan, A. Sasikumar, N. Senthilkumar, Res. Chem. Interm. **45**, 2657 (2019)
55. S. Vasantharaj, S. Sathiyavimal, P. Senthilkumar, F. LewisOscar, A. Pugazhendhi, J. Photochem. Photobiol. B **192**, 74 (2019)
56. M. Nasrollahzadeh, R. Akbari, Z. Issaabadi, S.M. Sajadi, Ceram. Int. **46**(2), 2093 (2020)
57. R. Hassanien, D.Z. Husein, M.F. Al-Hakkani, Heliyon **4**(12), e01077 (2018)
58. R. Hassanien, A.A. Abed-Elmageed, D.Z. Husein, Chem. Sel. **4**(31), 9018 (2019)